https://doi.org/10.5194/tc-2020-130
Preprint. Discussion started: 25 May 2020

The Cryosphere Discussions
Open Access
EGU

2020 Larsen C Ice Shelf surface melt is a 40-year record high

Suzanne Bevan[1], Adrian Luckman[1], Harry Hendon[2], and Guomin Wang[2]

[1]Geography Department, College of Science, Swansea University, Swansea SA2 8PP
[2]Bureau of Meteorology, Melbourne, Australia

Correspondence: Suzanne Bevan (s.l.bevan@swansea.ac.uk)

Abstract. Along with record-breaking summer air temperatures at two Antarctic Peninsula meteorological stations in February 2020, the Larsen C ice shelf experienced an exceptionally long and extensive 2019/2020 melt season. We use a 40-year time series of passive and scatterometer satellite microwave data, which is sensitive to the presence of liquid water in the snow pack, to reveal that the extent and duration of melt observed on the ice shelf in the austral summer of 2019/2020 was the greatest on record. We find that unusual perturbations to southern hemisphere modes of atmospheric flow, including a persistently positive Indian Ocean Dipole in the spring and a very rare southern hemisphere sudden stratospheric warming in September 2019, preceded the exceptionally warm Antarctic Peninsula summer. It is likely that teleconnections between the tropics and southern high latitudes were able to bring sufficient heat via the atmosphere and ocean to the Antarctic Peninsula to drive the extreme Larsen C Ice Shelf melt. The record breaking melt of 2019/2020 brought to an end the trend of decreasing melt that had begun in 1999/2000, and will reinitiate earlier thinning of the ice shelf by depletion of the firn air content.

1 Introduction

Surface melt and ponding on Antarctic Peninsula (AP) ice shelves has been linked to firn densification (Holland et al., 2011), surface lowering (Paolo et al., 2015), hydrofracture (Banwell et al., 2013), and eventual collapse (Scambos et al., 2000; van den Broeke, 2005). Following collapse the glaciers that feed the ice shelves have been observed to speed up (Gudmundsson, 2013), discharging more land ice to the oceans and increasing the rate of sea level rise. Larsen C Ice Shelf (LCIS, Fig 1) is the largest remaining ice shelf on the ~~peninsula~~ and surface melt and ponding have led to surface lowering, concentrated in the inlets and the northern parts of the shelf, and to the formation of a large subsurface mass of ice (Hubbard et al., 2016).

Satellite scatterometer data is sensitive to the presence of water within the snowpack and can be used to monitor melt on ice shelves (Barrand et al., 2013). Although positive degree days (one indicator of conditions favouring ice shelf surface melt) showed long-term increases from 1950 to 2010 (Barrand et al., 2013), between 2000 and 2016, a period dictated by the availability of scatterometer data, the number of melt days across the wider parts of LCIS decreased by 1 or 2 days per year (Bevan et al., 2018). However, spatial and interannual variability in melt is generally high and inlets (embayments adjacent to land) prone to localised föhn-induced melting (Luckman et al., 2014) continued to experience increasing annual melt.

The negative trend in melt duration on LCIS from 2000 to 2016 was in line with trends in AP air temperatures (Turner et al., 2016) and regional atmospheric circulation patterns, and coincided with a thickening and mass gain over most of the ice shelf (Adusumilli et al., 2018; Smith et al., 2020). In contrast to this trend, during the austral summer of 2019/2020 we observed

https://doi.org/10.5194/tc-2020-130
Preprint. Discussion started: 25 May 2020


The Cryosphere Discussions

a strong widespread fall in microwave backscatter across the shelf measured by Sentinel-1 synthetic aperture radar (SAR) indicating intense surface melt, and melt ponds could be seen in Cabinet Inlet in rare cloud-free visible imagery (Fig. 1).

It was also widely reported that air temperatures on 6 February 2020 reached a record (as yet unverified) of 18.4°C at Esperanza on the northern tip of the AP (public.wmo.int/en/media/news/new-record-antarctic-continent-reported). Three days later, on 9 February, 20.8°C was reported at Marambio on Seymour Island to the east of the AP. It seemed highly likely that the record-breaking air temperatures and extensive surface melt on LCIS were both manifestations of some atypical atmospheric circulation pattern.

In this study we present calculations of the duration and temporal evolution of the melt seasons on LCIS for summer 2019/2020 and the two previous summers, thereby extending published data (Bevan et al., 2018), and compare them with the melt seasons of the past 40 years. We then discuss the wider-scale meteorology, including tropical modes of flow and teleconnections, during austral spring and summer 2019/2020 in order to investigate why this year may have been so exceptional.

2 Methods and data

2.1 Melt analyses

Previous studies of AP ice-shelf melt have utilised daily enhanced resolution, 2.25 to 4.5 km, scatterometer data from Brigham Young University (Barrand et al., 2013; Bevan et al., 2018) where the Scatterometer Image Reconstruction (SIR) algorithm has been used to improve the spatial resolution of irregularly and oversampled data (Early and Long, 2001; Long and Hicks, 2010). However, these reconstructed products based on Quick Scatterometer (QuikSCAT, 1999-2009) and Advanced SCATterometer (ASCAT, 2009–present) data are not immediately available and are at the time of writing available only up to the end of 2018 (e.g. www.scp.byu.edu/data/Ascat/SIR/Ascat_sir.html). We update the SIR ASCAT melt estimates at 4.5 km resolution after Bevan et al. (2018) to include the 2017/2018 melt season. To continue the record to the present day we also produce an analysis of 2018/2019 and 2019/2020 over LCIS at a lower spatial resolution using ASCAT GDS Level 1 Sigma0 Swath Grid data from the EUMETSAT archive (archive.eumetsat.int/usc/).

ASCAT instruments currently operate onboard the METOPA, METOPB and METOPC satellites. However, as we want to derive a consistent melt product for the austral years of 2017/2018, 2018/2019 and 2019/2020 and METOPC was not launched until 7 November 2018 so we exclude data from this satellite from the study. The normalised backscatter data have an approximate spatial resolution of 15–30 km and are delivered on a 12.5 km grid.

The presence of water within the snowpack causes a sharp drop in microwave backscatter compared with cold dry snow. We record the presence of melt water at a pixel location when the backscatter is more than a carefully considered threshold below the previous winter (June, July, August) mean. In previous studies, using SIR data, the ASCAT (C band, 5.255 GHz) threshold was set at 2.7 dB (Ashcraft and Long, 2006; Bevan et al., 2018) and we use the same threshold with the Level 1 data. METOPA and METOPB observations over LCIS are acquired between 0200 and 0600, and between 0600 and 1000 local time, and we combine all mid-beam observations within a 24 hour period by taking the minimum backscatter value from all observations to maximise the chance of detecting melt. Melt days are then summed over the austral year August to July. We emphasise here

https://doi.org/10.5194/tc-2020-130
Preprint. Discussion started: 25 May 2020

that this method detects the presence of liquid water rather than the process of melting and that subsequent references to melt in the text should also be interpreted to mean the presence of liquid water.

We extend the analysis back from 1999 to 1979 using passive microwave data from the Scanning Multichannel Microwave Radiometer (SMMR, 1979–1987) and the Special Sensor Microwave/Imagers (SSM/I, 1989–2017), selecting the descending orbit 18.0 GHz and 19.35 GHz horizontally polarized channels, respectively (Picard and Fily, 2006). In a similar way to the scatterometer method we use a brightness temperature (T_b) threshold relative to the winter mean, which corresponds to the T_b−M method described in Ashcraft and Long (2006). Melt is detected when the daily T_b is more than 30 K above the previous winter mean (Picard and Fily, 2006). Time of day of overpass has been shown to have an impact on melt detection but the effect is not significant on the Antarctic Peninsula where melt is common and persistent. Choosing the descending passes for SMMR and SSMI minimizes the impact of instrument change (Picard and Fily, 2006) even if the overpass times are not at peak melt, and matches the ASCAT times more closely.

We use the detection of melt to calculate three measures. First, we calculate annual maps of melt duration by accumulating the total number of days of melt per year for each pixel. These datasets are then resampled to a 2 km grid and masked to the ice-shelf area which includes Larsen D but excludes the Larsen C area that calved in July 2017. Second, we calculate the total area of ice shelf melt per day, and third we calculate melt indices to enable a quantitative interannual comparison of melt over the whole ice shelf. The melt index is the product of the number of melt days per pixel times the pixel area, summed over the area of LCIS.

There are two periods of Level 1 ASCAT data missing in the newly analysed period: 22 days from 12/12/2017 to 02/01/2018, and 30 days from 17/12/2018 to 15/01/2019. We assess how much the data gaps might lead to underestimates of melt by calculating the melt indices for these short periods using the SIR ASCAT data for the equivalent periods in 2017/2018.

2.2 Atmospheric circulation

The evolution of the atmospheric circulation during austral spring-summer 2019-2020 and a comparison to historical variability are described using the ERA5 reanalyses (Copernicus Climate Change Service (C3S) (2017): ERA5: Fifth generation of ECMWF atmospheric reanalyses of the global climate. cds.climate.copernicus.eu/cdsapp#!/home). We use monthly mean pressure-level heights and daily 2 m air temperatures. These data are available on ∼30 km grid and cover the period January 1979–March 2020. Sea ice concentrations were downloaded from the National Snow and Ice Data Center (NSIDC) and are available as monthly means on a 25 km grid for January 1981–March 2020. Sea surface temperatures (SSTs) are the NOAA Optimal Interpolation SST v2 data (Reynolds et al., 2002). These data are available as weekly means on a 1 degree grid and are available January 1982–March 2020.

The Indian Ocean Dipole (IOD) is the Indian Ocean equivalent of an El Niño and its phase (Dipole Model Index, DMI) is calculated as the difference in SST anomalies between two regions of the Indian Ocean (Wang et al., 2019). We use the DMI to indicate how tropical weather patterns were having an effect on higher latitudes.

We monitor the latitudinal position of the high latitude westerly jet using the Southern Annular Mode index (Marshall, 2003). The SAM index is the difference in zonal mean surface pressure at 40°S and 65°S. A positive value of the index indicates a

https://doi.org/10.5194/tc-2020-130
Preprint. Discussion started: 25 May 2020

strengthened and poleward shifted westerly jet while a negative value indicates a weakened and equatorward shifted westerly jet. Historically, high SAM (southward displacement of the westerly jet) is associated with warming on the east (leeward) side of the Antarctic Peninsula (Thompson and Wallace, 2000) due to föhn winds and local southerly advection of warmer air from the north.

3 Results

Comparing the maps of melt on LCIS (Fig. 2) with Bevan et al. (2018, Fig. 6) we can see that the 2017/2018 melt based on Level 1 ASCAT data compares well with the SIR data. Melt in 2018/2019 is very low in contrast to melt in 2019/2020 which appears to be particularly intense. Melt distribution follows the typical pattern of enhanced melt in the inlets close to the mountains superimposed on a general south to north gradient of increasing melt (Bevan et al. (2018, Fig. 6) and Fig. A1). Inspection of daily images of backscatter (not presented) shows that patches of melt, mostly focussed on the inlets close to the mountains begins in October 2019, but from January 2020 through February and into March the entire ice shelf has very low backscatter indicating the persistent presence of liquid water.

The temporal evolution of melt area shows intermittent melt episodes during the last 4 months of 2019, not dissimilar to previous years, followed by a steep increase from early January 2020 that persisted until the end of March (Fig. 4). This persistence of large areas of melt is very unusual in comparison with the previous 20 years with the exception of 2002/2003 (highlighted in blue in Fig. 4).

The time series of melt indices (Fig. 3) confirms the exceptional nature of 2019/2020 — the melt index in 2019/2020 at 6.0×10^6 melt days km^2 is the highest in the record. Based on the SIR ASCAT data for 2017/2018 the melt indices for the short 22- and 30-day periods when Level 1 ASCAT data in 2017/2018 and 2018/2019 are missing, are only 0.17 and 0.34×10^6 melt days km^2, respectively. ie. the majority of melt happens later in summer. The 22-day figure suggests that the melt index for 2017/2018 based on Level 1 ASCAT data of 0.80×10^6 melt days km^2 is not greatly underestimated because of the missing data, and the good agreement between SIR and Level 1 melt indices shown in Fig. 3 can be trusted. The 30 day figure, whilst for the previous year, suggests that the low melt index for 2018/2019 of 0.22×10^6 melt days km^2 may be as high as 0.56×10^6 melt days km^2 which would still be the lowest on record.

The ERA5 2 m air temperatures (Fig. 5) show repeated intervals of anomalously warm air over the ice shelf but that it was not until late December or early January 2020 that air temperatures were consistently above -2°C and anomalously warm. Melt is able to occur and persist above -2°C as surface energy budget calculations on LCIS have shown that surface temperatures can exceed 2 m temperatures by up to 2°C under calm cloudy conditions (Kuipers Munneke et al., 2012). In addition Fig. 5 shows the mean daily temperature, it is very likely that temperatures were higher for a large part of the day.

Turning to the indices of atmospheric flow, a very strong positive IOD began in winter and was matured during austral spring (August–November 2019), peaking at over 3 standard deviations above the mean in October 2019, making it one of the strongest IODs on record (Fig. 6). Monthly SAM indices for October 2019 to December 2019 were strongly negative at -1.97, -4.42, -1.78, but in January, February and March increased to 0.57, -0.36 and 2.05.

https://doi.org/10.5194/tc-2020-130
Preprint. Discussion started: 25 May 2020

4 Discussion

The Level 1 ASCAT data have allowed a rapid but robust assessment of the two most recent LCIS 2019/2020 melt seasons, with the SIR/Level 1 overlap period of 2017/2018 allowing a validation of the duration and location of melt derived from Level 1 data. The analysis shows that melt durations in 2018/2019 and 2019/2020 were at the extreme ends of that observed on LCIS since 1979. In 2018/2019, melt appears to continue the general trend of decreasing melt that began in the early 2000s and the melt index was the lowest on record. In 2019/2020 intense and widespread melt covered the ice shelf, in a manner not observed since 2002/2003 (Bevan et al., 2018).

The large-scale atmospheric flow leading up to and through the extreme melt season in 2019/2020 consists of a sequence of unusual events. A very strong IOD developed in winter and persisted through early summer 2019 (Fig. 6). Historically, a positive IOD during austral spring acts to excite a stationary Rossby wave train into the Southern Hemisphere extratropics, which places an anticyclone to the south-west of Cape Horn (Fig. A2d). The associated southerly surface winds near and to the east of the AP produce colder than normal air temperatures (Fig. A3d) and an increase in sea ice concentration in the Weddell Sea (Fig. A4d). Similarly, to the west of the Peninsula, the positive IOD typically acts to drive northerly surface winds that act to warm the surface and decrease sea ice in the Bellingshausen Sea. The observed anomalies of circulation in the lower troposphere, and the air temperatures and sea ice concentration during August–September 2019 (Figs. A2a, A3a, and A4a) match well with what typically occurs during a positive IOD event.

However, in early September 2019, a sudden stratospheric warming (SSW) occurred, which was historically early and of comparable magnitude to the only previous major sudden stratospheric warming that occurred in late September 2002 (Lim et al. 2020, SPARC, 2019: SPARC Newsletter No. 54, January 2020, 48 pp., available at www.sparc-climate.org/publications/newsletter) when, intriguingly, the summer melt on LCIS was also exceptionally high (Figs. 3 and 4). SSWs weaken or even completely reverse the westerly stratospheric polar jets and generate extreme weather events throughout the polar and subpolar regions of the Southern Hemisphere in the following months as the weakened or reversed vortex descends to the surface resulting in low SAM. The coupling of the 2019 SSW to the surface triggered persistent record negative SAM from the 3rd week of October through the end of December.

As a result of the SSW and development of negative SAM, we might have anticipated a further increase of sea ice and strengthening of the cold conditions on and east of the AP during November and December that had been generated earlier by the positive IOD. However, the swing to negative SAM altered the mean flow through which the IOD-forced stationary Rossby wave train was propagating. The easterly anomalies in the high latitudes acted to more strongly refract the IOD-forced Rossby wave train back to the Tropics (Fig. A2b). The net effect is that from late October through to the end of December, while the IOD event was, unusually, persisting and the SAM was strongly negative, a cyclone replaced the anticyclone to the west of the AP (Fig. A2b). The resulting northwesterly and northeasterly flow on either side of the AP acted to warm the surface, remove the enhanced sea ice in the Weddell sea (Fig. A4b), and drive southward Ekman transport of warm SSTs towards the AP (Fig. A5b and c).

https://doi.org/10.5194/tc-2020-130
Preprint. Discussion started: 25 May 2020

The preceding events were undoubtedly unusual and by delivering broad-scale ocean heat to the region by the end of December were likely to have acted as important precursors to the anomalously high presence of melt during January and February. Although the influence of the IOD and SSW on the circulation disappeared by the end of December, during late summer an anticyclone was established over the AP (positive 500 hPa geopotential height anomaly, Fig. A2c) resulting in poleward surface flow that tapped into the ocean heat, keeping air temperatures high on the AP as featured in station observations and ERA5 2 m air temperatures (Fig. 5). Two factors will have contributed to the continued detection of surface melt into March 2020. Firstly, during summer short wave radiation is able to penetrate the snow pack, particularly when the surface is at or near melting (Kuipers Munneke et al., 2012), causing subsurface melt. Secondly, microwaves are also able to penetrate the snow pack so that reductions in backscatter due to absorption are sensitive to subsurface as well as surface liquid water. In other words, the persistence of subsurface melt water following extreme and prolonged surface melt will have contributed to the scatterometer derived melt area. This effect also reduces the impact of the less than optimal overpass times for the passive microwave and ASCAT observations of melt on LCIS.

This record ice-shelf wide melt following a period low SAM indices and weakened westerlies at first seems to contradict observations that strong westerlies enhance föhn warming and subsequent melt on eastern AP ice shelves. However, we note that in extreme melt years such as 2019/2020 the melt extends across the full width of the shelf, but that the deep föhn events required to produce melt this far from the mountains (Elvidge et al., 2015) are relatively rare (Cape et al., 2015). In addition, the temperature anomalies produced by föhn events are much smaller during the summer than other seasons (Kuipers Munneke et al., 2018; Wiesenekker et al., 2018) and account for a smaller proportion of melt.

It is likely that the record high 2019/2020 melt index we have observed on Larsen C Ice Shelf will also have been experienced elsewhere in the region.

5 Conclusions

The 2019/2020 LCIS melt season was longer and more intense than any observed over the last 40 years, bringing to an abrupt halt the apparent 21st century decline in surface melt. The extreme melt through the summer of 2020 is likely to have reinitiated thinning of the entire ice shelf through loss of firn air content. Although late winter and early spring 2019 were cold on and around the AP as expected under a strong positive IOD, this was interrupted by an SSW which caused the ongoing IOD to bring warmth to the region in December and into January when normally the low SAM indices would have meant cold conditions. The majority of the 2019/2020 melt was detected in January to March 2020 probably as a result of anticyclonic conditions over the shelf drawing on abnormally warm and ice-free surrounding oceans. Even once the actual process of melt had ceased, the liquid water was likely able to persist within suburface layers and hence be detected by scatterometer.

These atypical atmospheric phenomena are indications of how tropical and extratropical weather patterns can impact high latitudes. Further investigation into these teleconnections and the implications for future ice-shelf stability is an important area for continued research. Surface energy budget modelling on LCIS would also be able to shed light on the exact balance of fluxes contributing to the melt.

https://doi.org/10.5194/tc-2020-130
Preprint. Discussion started: 25 May 2020

Data availability. The NERC Polar Data Centre hosts Geotiffs of melt duration based on the SIR QuikSCAT/ASCAT and Level 1 ASCAT data (doi.org/10.5285/e3616d28-759e-4cca-8fae-fe398f9552ba (Bevan and Luckman, 2018),
195 and doi.org/10.5285/cfa4cc5d-3ea9-4c3c-8d6b-6b92a81bb2af (Bevan and Luckman, 2020), respectively).

Author contributions. SB analysed the satellite data and drafted the manuscript. AL authored the code to retrieve melt duration and contributed to writing the manuscript. HH and GW advised on the meteorological discussions and produced Figs. 5 and 6, and Figs. A2 to A5.

Competing interests. The authors declare that they have no conflicts of interest.

200 *Acknowledgements.* Thanks to EUMETSAT for the Level 1 ASCAT data, and to Brigham Young University Microwave Remote Sensing Unit for the enhanced SIR QuikSCAT and ASCAT data. The Nimbus-7 SMMR Pathfinder Daily EASE-Grid Brightness Temperatures, Version 1 (Knowles et al., 2000), and DMSP SSM/I-SSMIS Pathfinder Daily EASE-Grid Brightness Temperatures, Version 2 (Armstrong et al., 1994) were downloaded from the NSIDC. NSIDC also supplied the sea ice concentration data (Cavalieri, D. J., C. L. Parkinson, P. Gloersen, and H. J. Zwally. 1996, updated yearly. Sea Ice Concentrations from Nimbus-7 SMMR and DMSP SSM/I-SSMIS Pas-
205 sive Microwave Data, Version 1. Boulder, Colorado USA. NASA National Snow and Ice Data Center Distributed Active Archive Center. doi.org/10.5067/8GQ8LZQVL0VL. [April, 2020].). The ERA5 data were made available by the Copernicus Atmosphere Monitoring Service information [2020], neither the European Commission nor ECMWF is responsible for any use that may be made of the Copernicus information or data it contains. SAM index data were obtained from the British Antarctic Survey (www.nerc-bas.ac.uk/icd/gjma/sam.html). SB was funded by NERC grant NE/L005409/1.

https://doi.org/10.5194/tc-2020-130
Preprint. Discussion started: 25 May 2020

References

Adusumilli, S., Fricker, H. A., Siegfried, M. R., Padman, L., Paolo, F. S., and Ligtenberg, S. R. M.: Variable Basal Melt Rates of Antarctic Peninsula Ice Shelves, 1994–2016, Geophysical Research Letters, 45, 4086–4095, https://doi.org/10.1002/2017GL076652, 2018.

Armstrong, R., Knowles, K., Brodzik, M. J., and Hardman, M. A.: DMSP SSM/I-SSMIS Pathfinder Daily EASE-Grid Brightness Temperatures, Version 2. Boulder, Colorado USA. NASA National Snow and Ice Data Center Distributed Active Archive Center., https://doi.org/10.5067/3EX2U1DV3434, 1994.

Ashcraft, I. S. and Long, D. G.: Comparison of methods for melt detection over Greenland using active and passive microwave measurements, International Journal of Remote Sensing, 27, 2469–2488, https://doi.org/10.1080/01431160500534465, 2006.

Banwell, A. F., MacAyeal, D. R., and Sergienko, O. V.: Breakup of the Larsen B Ice Shelf triggered by chain reaction drainage of supraglacial lakes, Geophysical Research Letters, 40, 5872–5876, https://doi.org/10.1002/2013GL057694, _eprint: https://agupubs.onlinelibrary.wiley.com/doi/pdf/10.1002/2013GL057694, 2013.

Barrand, N. E., Vaughan, D. G., Steiner, N., Tedesco, M., Kuipers Munneke, P., van den Broeke, M. R., and Hosking, J. S.: Trends in Antarctic Peninsula surface melting conditions from observations and regional climate modeling, J. Geophys. Res. Earth Surf., 118, 315–330, https://doi.org/10.1029/2012jf002559, 2013.

Bevan, S. and Luckman, A.: Annual melt onset, duration and end dates for the Antarctic Peninsula derived from Quikscat and ASCAT scatterometer Enhanced Resolution data, 1999-2017, Discovery Metadata System, https://doi.org/10.5285/E3616D28-759E-4CCA-8FAE-FE398F9552BA, 2018.

Bevan, S. and Luckman, A.: Antarctic Peninsula melt season durations based on level 1 ASCAT scatterometer data, 2017-2020, Discovery Metadata System, https://doi.org/10.5285/CFA4CC5D-3EA9-4C3C-8D6B-6B92A81BB2AF, 2020.

Bevan, S. L., Luckman, A. J., Kuipers Munneke, P., Hubbard, B., Kulessa, B., and Ashmore, D. W.: Decline in Surface Melt Duration on Larsen C Ice Shelf Revealed by The Advanced Scatterometer (ASCAT), Earth and Space Science, 5, 578–591, https://doi.org/10.1029/2018ea000421, 2018.

Cape, M. R., Vernet, M., Skvarca, P., Marinsek, S., Scambos, T., and Domack, E.: Foehn winds link climate-driven warming to ice shelf evolution in Antarctica, J. Geophys. Res. Atm., 120, 11,037–11,057, https://doi.org/10.1002/2015jd023465, 2015.

Early, D. S. and Long, D. G.: Image reconstruction and enhanced resolution imaging from irregular samples, IEEE Transactions on Geoscience and Remote Sensing, 39, 291–302, https://doi.org/10.1109/36.905237, 2001.

Elvidge, A. D., Renfrew, I. A., King, J. C., Orr, A., Lachlan-Cope, T. A., Weeks, M., and Gray, S. L.: Foehn jets over the Larsen C Ice Shelf, Antarctica, Q.J.R. Meteorol. Soc., 141, 698–713, https://doi.org/10.1002/qj.2382, 2015.

Gudmundsson, G. H.: Ice-shelf buttressing and the stability of marine ice sheets, The Cryosphere, 7, 647–655, https://doi.org/https://doi.org/10.5194/tc-7-647-2013, publisher: Copernicus GmbH, 2013.

Haran, T., Bohlander, J., Scambos, T., Painter, T., and Fahnestock, M.: MODIS Mosaic of Antarctica 2008-2009 (MOA2009) Image Map, Version 1, Boulder, Colorado USA.NSIDC: National Snow and Ice Data Center, http://nsidc.org/data/NSIDC-0593, 2014.

Holland, P. R., Corr, H. F. J., Pritchard, H. D., Vaughan, D. G., Arthern, R. J., Jenkins, A., and Tedesco, M.: The air content of Larsen Ice Shelf, Geophys. Res. Lett., 38, L10 503+, https://doi.org/10.1029/2011gl047245, 2011.

Hubbard, B., Luckman, A., Ashmore, D. W., Bevan, S., Kulessa, B., Kuipers Munneke, P., Philippe, M., Jansen, D., Booth, A., Sevestre, H., Tison, J.-L., O'Leary, M., and Rutt, I.: Massive subsurface ice formed by refreezing of ice-shelf melt ponds, Nat. Commun., 7, 11 897+, https://doi.org/10.1038/ncomms11897, 2016.

https://doi.org/10.5194/tc-2020-130
Preprint. Discussion started: 25 May 2020

Knowles, K., Njoku, E. G., Armstrong, R., and Brodzik, M. J.: Nimbus-7 SMMR Pathfinder Daily EASE-Grid Brightness Temperatures, Version 1. Boulder, Colorado USA. NASA National Snow and Ice Data Center Distributed Active Archive Center, https://doi.org/10.5067/36SLCSCZU7N6, 2000.

Kuipers Munneke, P., van den Broeke, M. R., King, J. C., Gray, T., and Reijmer, C. H.: Near-surface climate and surface energy budget of Larsen C ice shelf, Antarctic Peninsula, The Cryosphere, 6, 353–363, https://doi.org/10.5194/tc-6-353-2012, 2012.

Kuipers Munneke, P., Luckman, A. J., Bevan, S. L., Smeets, C. J. P. P., Gilbert, E., van den Broeke, M. R., Wang, W., Zender, C., Hubbard, B., Ashmore, D., Orr, A., and King, J. C.: Intense Winter Surface Melt on an Antarctic Ice Shelf, Geophysical Research Letters, 45, 7615–7623, https://doi.org/10.1029/2018gl077899, 2018.

Long, D. G. and Hicks, B. R.: Standard BYU QuikSCAT and Seawinds Land/Ice Image Products, Tech. rep., BYU Center for Remote Sensing, Microwave Earth Remote Sensing Laboratory, BYU Center for Remote Sensing, Brigham Young University, 459 Clyde Building, Provo, UT 84602, http://www.scp.byu.edu/docs/EnhancedFAQ.html, 2010.

Luckman, A., Elvidge, A., Jansen, D., Kulessa, B., Munneke, P. K., King, J., and Barrand, N. E.: Surface melt and ponding on Larsen C Ice Shelf and the impact of föhn winds, Antarct. Sci., 26, 625–635, https://doi.org/10.1017/s0954102014000339, 2014.

Marshall, G. J.: Trends in the Southern Annular Mode from Observations and Reanalyses, Journal of Climate, 16, 4134–4143, https://doi.org/10.1175/1520-0442(2003), 2003.

Paolo, F. S., Fricker, H. A., and Padman, L.: Volume loss from Antarctic ice shelves is accelerating, Science, 348, 327–331, https://doi.org/10.1126/science.aaa0940, 2015.

Picard, G. and Fily, M.: Surface melting observations in Antarctica by microwave radiometers: Correcting 26-year time series from changes in acquisition hours, Remote Sensing of Environment, 104, 325–336, https://doi.org/10.1016/j.rse.2006.05.010, 2006.

Reynolds, R. W., Rayner, N. A., Smith, T. M., Stokes, D. C., and Wang, W.: An Improved In Situ and Satellite SST Analysis for Climate, Journal of Climate, 15, 1609–1625, https://doi.org/10.1175/1520-0442(2002)015<1609:AIISAS>2.0.CO;2, publisher: American Meteorological Society, 2002.

Scambos, T. A., Hulbe, C., Fahnestock, M., and Bohlander, J.: The link between climate warming and break-up of ice shelves in the Antarctic Peninsula, J. Glaciol., pp. 516–530, https://doi.org/10.3189/172756500781833043, 2000.

Smith, B., Fricker, H. A., Gardner, A. S., Medley, B., Nilsson, J., Paolo, F. S., Holschuh, N., Adusumilli, S., Brunt, K., Csatho, B., Harbeck, K., Markus, T., Neumann, T., Siegfried, M. R., and Zwally, H. J.: Pervasive ice sheet mass loss reflects competing ocean and atmosphere processes, Science, https://doi.org/10.1126/science.aaz5845, publisher: American Association for the Advancement of Science Section: Report, 2020.

Thompson, D. W. J. and Wallace, J. M.: Annular Modes in the Extratropical Circulation. Part I: Month-to-Month Variability, Journal of Climate, 13, 1000–1016, https://doi.org/10.1175/1520-0442(2000)013<1000:AMITEC>2.0.CO;2, publisher: American Meteorological Society, 2000.

Turner, J., Lu, H., White, I., King, J. C., Phillips, T., Hosking, J. S., Bracegirdle, T. J., Marshall, G. J., Mulvaney, R., and Deb, P.: Absence of 21st century warming on Antarctic Peninsula consistent with natural variability, Nature, 535, 411–415, https://doi.org/10.1038/nature18645, 2016.

van den Broeke, M.: Strong surface melting preceded collapse of Antarctic Peninsula ice shelf, Geophys. Res. Lett., 32, L12 815+, https://doi.org/10.1029/2005gl023247, 2005.

https://doi.org/10.5194/tc-2020-130
Preprint. Discussion started: 25 May 2020

Wang, G., Hendon, H. H., Arblaster, J. M., Lim, E.-P., Abhik, S., and Rensch, P. v.: Compounding tropical and stratospheric forcing of the record low Antarctic sea-ice in 2016, Nature Communications, 10, 1–9, https://doi.org/10.1038/s41467-018-07689-7, number: 1 Publisher: Nature Publishing Group, 2019.

Wiesenekker, J. M., Kuipers Munneke, P., Van den Broeke, M. R., and Smeets, C. J. P. P.: A Multidecadal Analysis of Föhn Winds over Larsen C Ice Shelf from a Combination of Observations and Modeling, Atmosphere, 9, 172, https://doi.org/10.3390/atmos9050172, number: 5 Publisher: Multidisciplinary Digital Publishing Institute, 2018.

https://doi.org/10.5194/tc-2020-130
Preprint. Discussion started: 25 May 2020

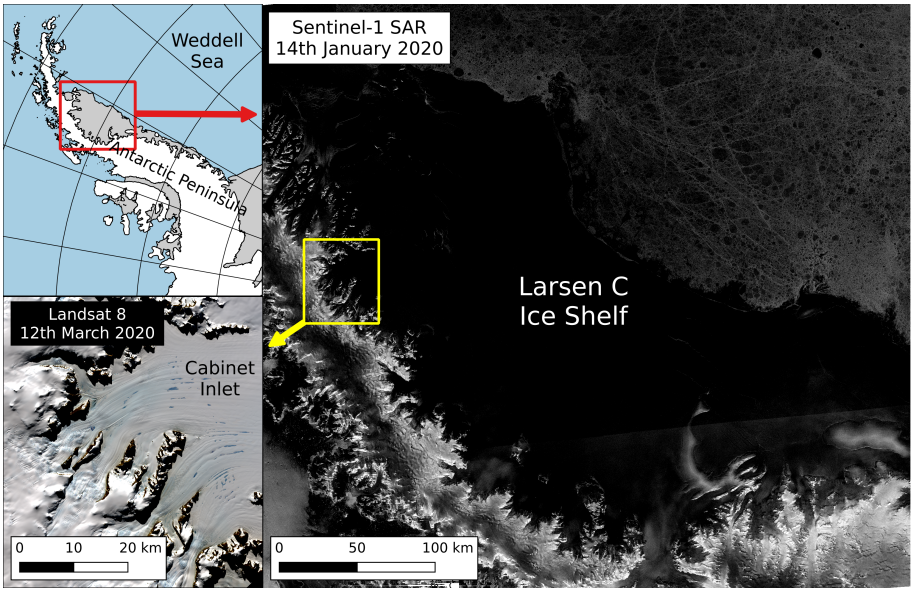

Figure 1. Copernicus Sentinel-1 synthetic aperture radar (SAR) image (processed by the European Space Agency) showing widespread low backscatter on Larsen C Ice Shelf and (inset) melt ponds in Cabinet Inlet visible in a Landsat 8 image (courtesy of the U.S. Geological Survey). Coastline and grounding line were obtained from the NSIDC (Haran et al., 2014).

https://doi.org/10.5194/tc-2020-130
Preprint. Discussion started: 25 May 2020

The Cryosphere Discussions
Open Access
EGU

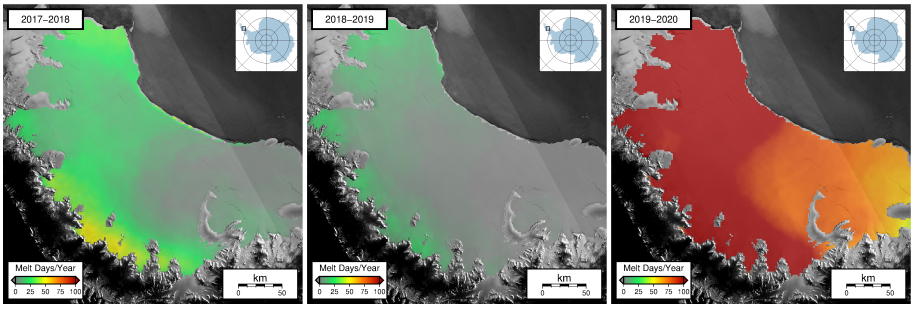

Figure 2. Number of melt days in the three most recent melt seasons, calculated using Level 1 ASCAT data. The background image is Copernicus Sentinel-1 2019 mean backscatter.

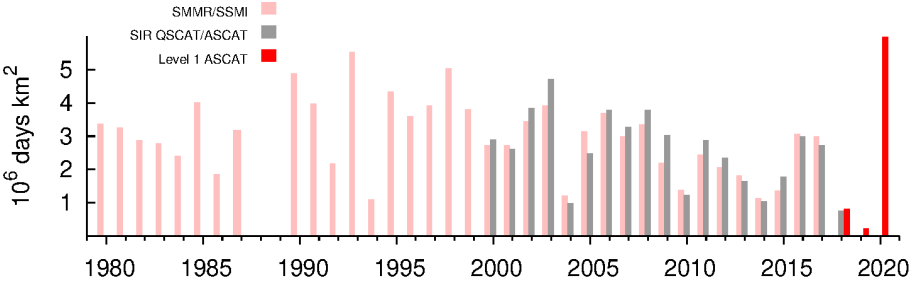

Figure 3. Melt index time series based on brightness temperatures from SMMR and SSMI, SIR QuikSCAT and ASCAT data, and Level 1 ASCAT data.

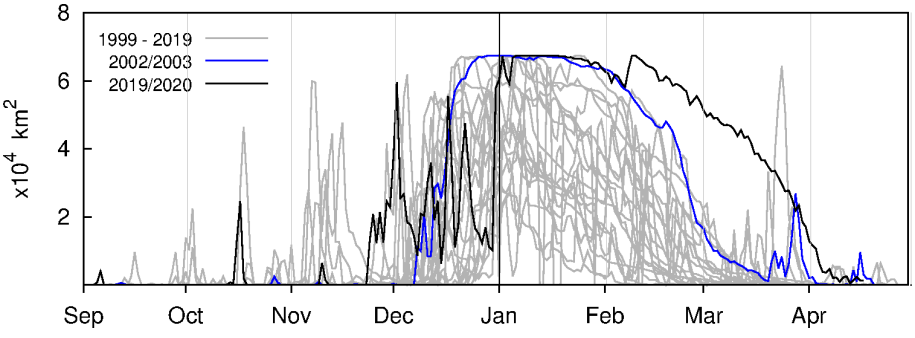

Figure 4. Ice shelf melt area. The 1999-2019 curves are based on the three sets of scatterometer data, QuikSCAT, SIR ASCAT and Level 1 ASCAT.

https://doi.org/10.5194/tc-2020-130
Preprint. Discussion started: 25 May 2020

The Cryosphere
Discussions
Open Access
EGU

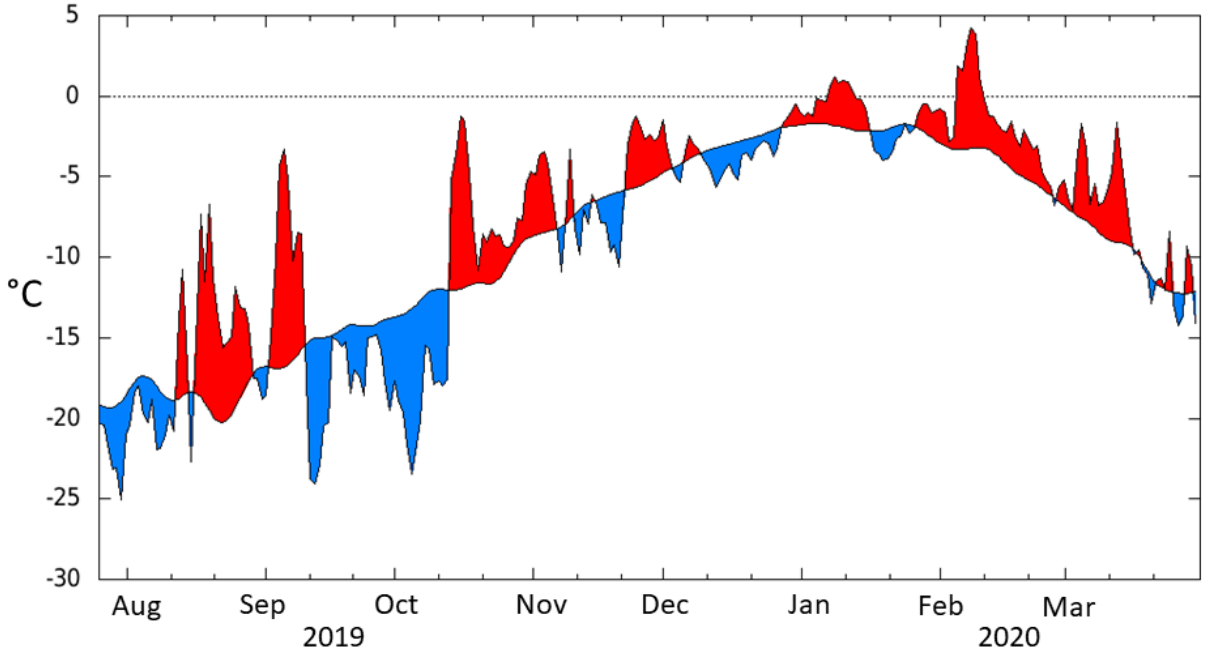

Figure 5. Mean daily and 1979–2019 mean ERA5 2 m air temperatures averaged over the area 60 to 65°W, −65 to −70°N. Positive (negative) anomalies are shaded red (blue).

https://doi.org/10.5194/tc-2020-130
Preprint. Discussion started: 25 May 2020

The Cryosphere
Discussions
Open Access
EGU

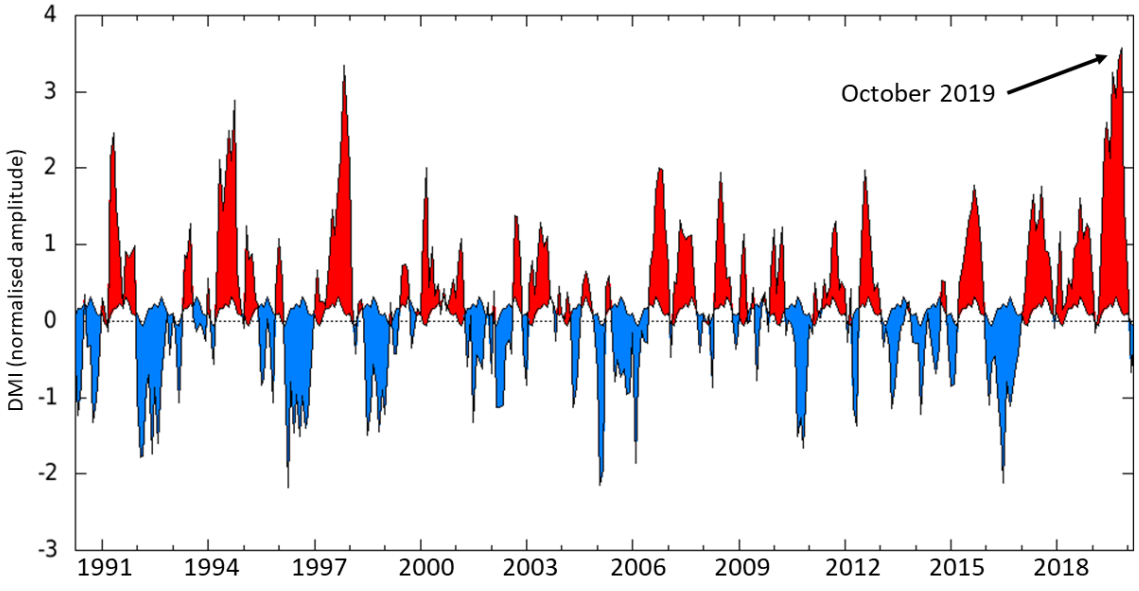

Figure 6. Standardized time series of the Dipole Mode Index (difference between the SST averaged in the western equatorial Indian Ocean (50°E–70°E and 10°S–10°N) and the south eastern equatorial Indian Ocean (90°E–110°E and 10°S–0°N) based on Extended Reconstructed Sea Surface Temperature data (ERSST, www.ncdc.noaa.gov/data-access/marineocean-data/extended-reconstructed-sea-surface-temperature-ersst-v5).

https://doi.org/10.5194/tc-2020-130
Preprint. Discussion started: 25 May 2020

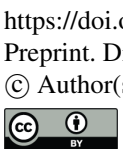

The Cryosphere
Discussions
Open Access
EGU

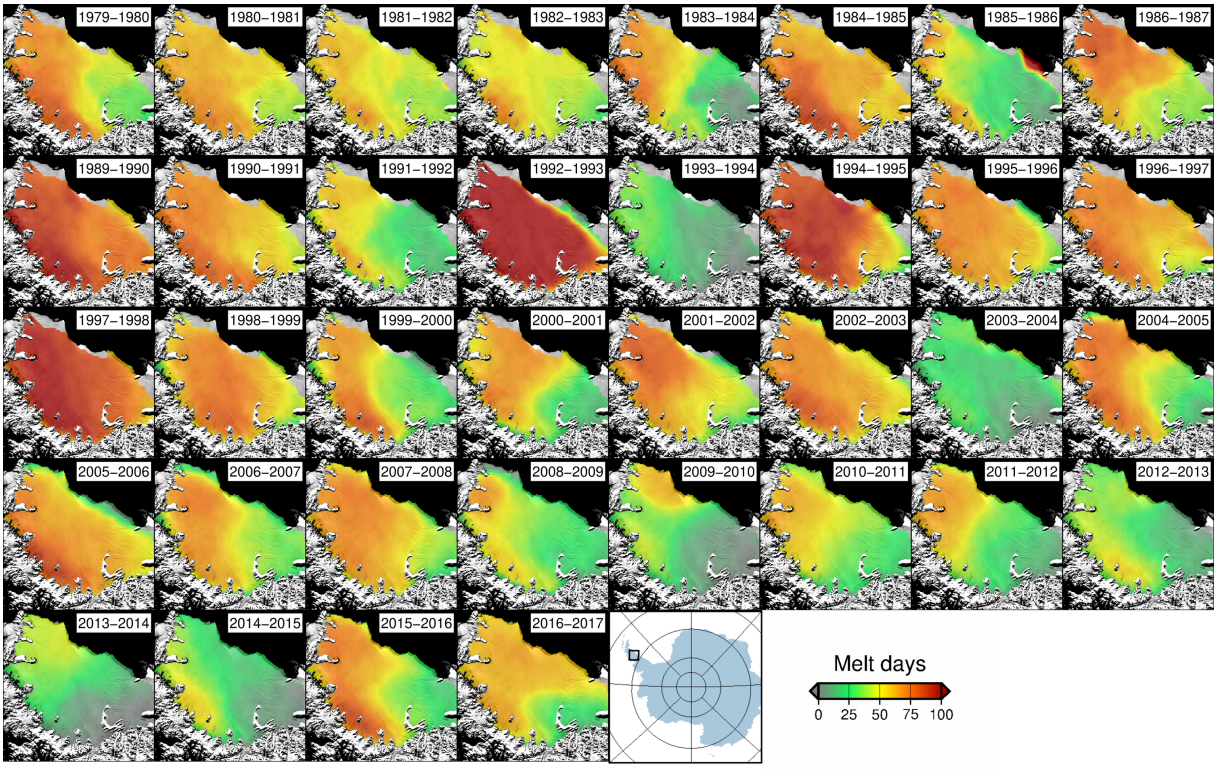

Figure A1. Time sequence of annual melt duration based on passive microwave data(SMMR, 1979–1987 and SSM/I, 1989–2017). Summers 1987/1988 and 1988/1989 are missing due to data unavailability.

https://doi.org/10.5194/tc-2020-130
Preprint. Discussion started: 25 May 2020

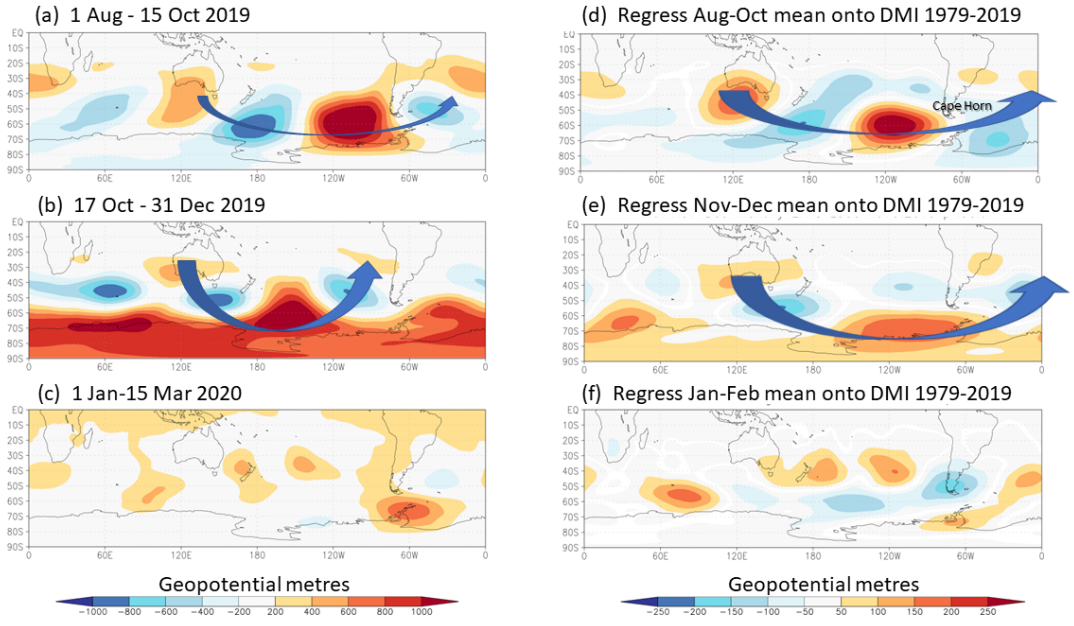

Figure A2. Left panels: Anomalies in ERA5 500 hPa geopotential height relative to the 1979–2019 climatological mean for a) 1 August to 15 October 2019, b) 17 October to 31 December 2019, c) 1 January to 15 March 2020. The averaging periods were shifted slightly to maximize signals observed in 2019/2020. Right panels: Linear regression of the geopotential height anomaly onto the Dipole Mode Index (DMI) for the equivalent period based on data from 1979 to 2019. The regression coefficients are scaled by 1 standard deviation of the DMI so that the maps represent the height anomaly that would be accounted for by 1 standard deviation in DMI for d) August to October, e) November to December, f) January to February. The blue arrows depict the Rossby wave train ray path and highlight the shortening of the Rossby wavelength in November/December 2019.

https://doi.org/10.5194/tc-2020-130
Preprint. Discussion started: 25 May 2020

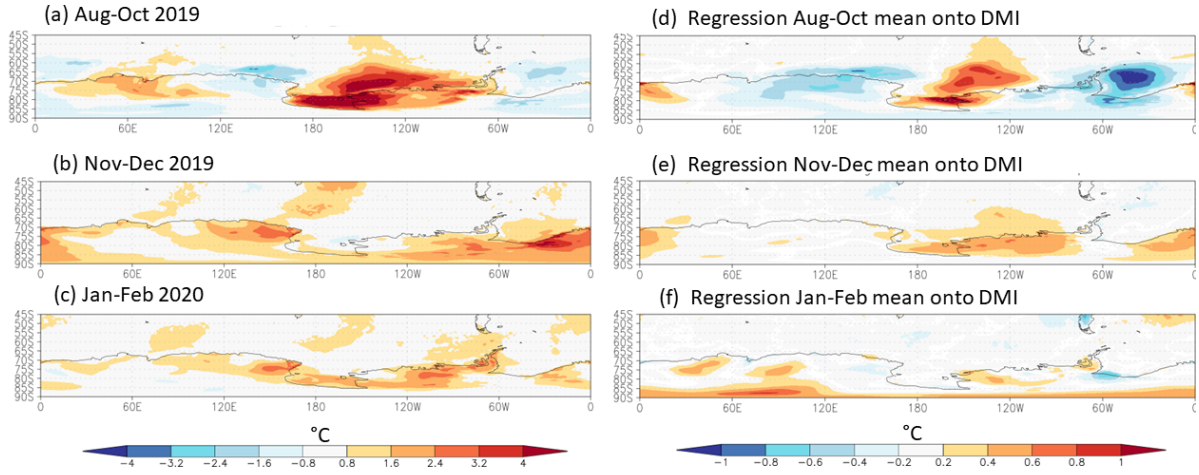

Figure A3. Left panels: Anomalies in ERA5 2 m air temperatures relative to the 1979–2019 climatological mean for a) August, September and October 2019, b) November and December 2019, c) January and February 2020. Right panels: Linear regression of 2 m temperature anomaly onto the Dipole Mode Index (DMI) for the equivalent period based on data from 1979 to 2019. The regression coefficients are scaled by 1 standard deviation of the DMI so that the maps represent the temperature anomaly that would be accounted for by 1 standard deviation in DMI for d) August to October, e) November to December, f) January to February.

https://doi.org/10.5194/tc-2020-130
Preprint. Discussion started: 25 May 2020

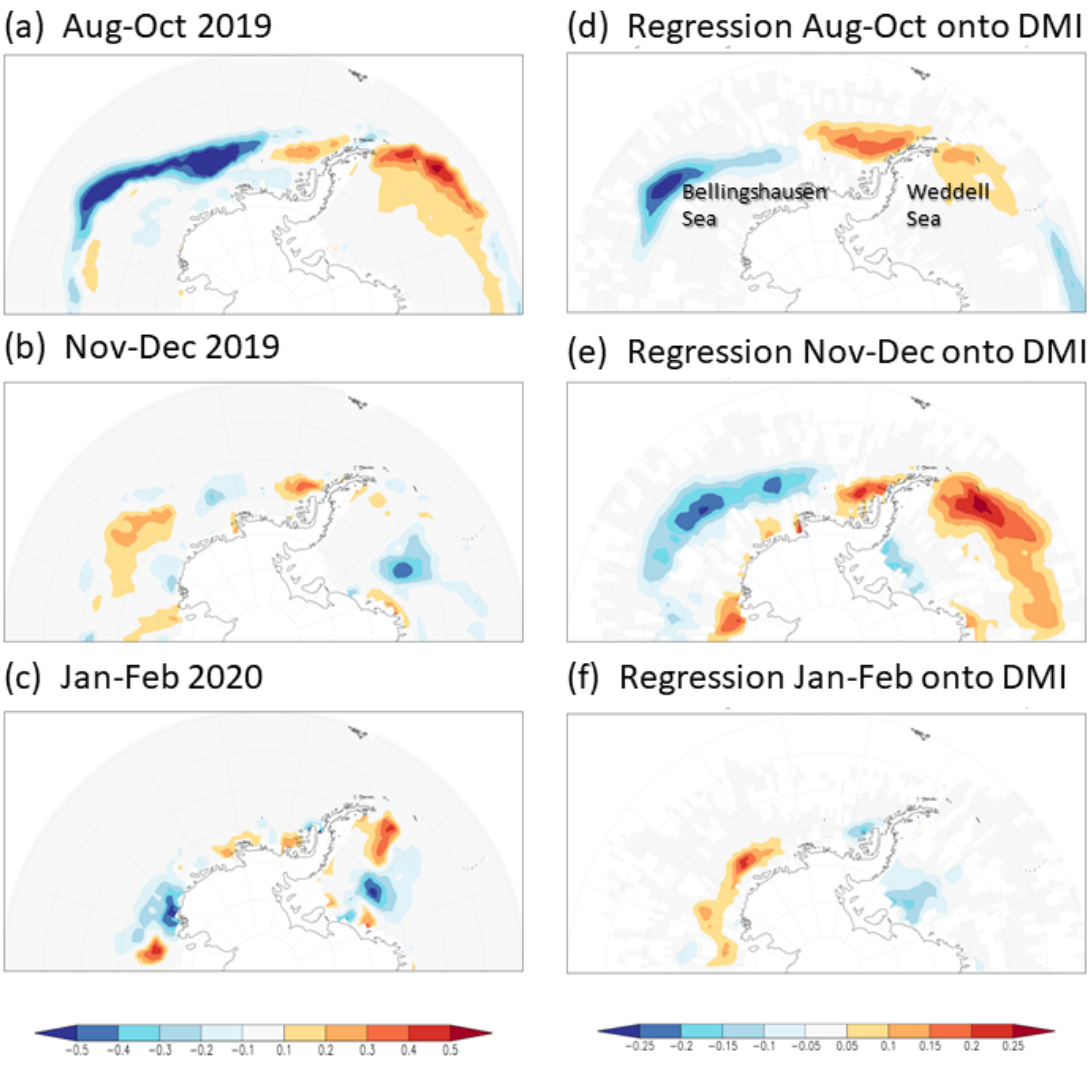

Figure A4. Left panels: Anomaly in sea ice concentration relative to the 1981 to 2019 mean for a) August, September and October 2019, b) November and December 2019, c) January and February 2020. Right panels: Linear regression of sea ice concentration anomaly onto the Dipole Mode Index (DMI) for the equivalent period based on data from 1981 to 2019. The regression coefficients are scaled by 1 standard deviation of the DMI so that the maps represent the sea ice anomaly that would be accounted for by 1 standard deviation in DMI for d) August to October, e) November to December, f) January to February.

https://doi.org/10.5194/tc-2020-130
Preprint. Discussion started: 25 May 2020

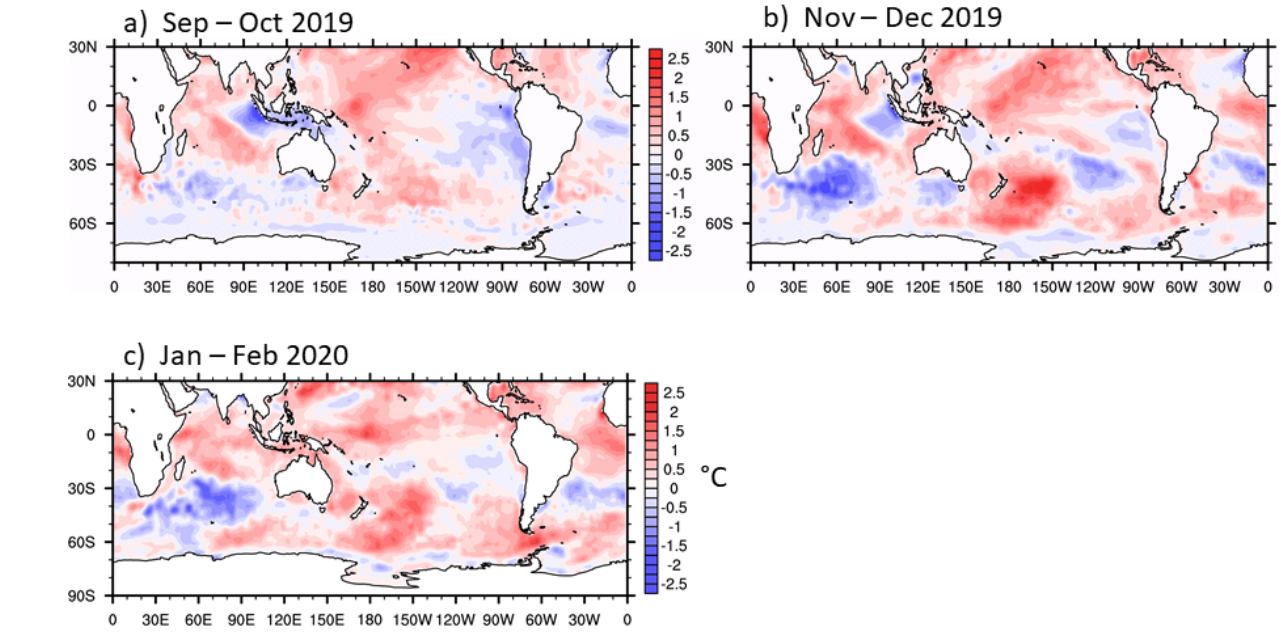

Figure A5. Sea surface temperature (SST) anomalies relative to 1982–2019 mean for a) September and October 2019, b) November and December 2019, c) January and February 2020. SST data are NOAA OI v2.